very close to the previous NASA results with a slight delay in the prediction of transition.

Conclusions

The objective of this research was to implement a highly accurate numerical method and combine an analytical heating analysis that can be integrated together to predict heating rates on hypersonic vehicles. The motivation for this research project was the need for accurate prediction of aerodynamic heating around hypersonic vehicles. New grid-generation routines were developed that enable the definition of a generic hypersonic vehicle surface. Complex three-dimensional geometries that include wing and tail sections can now be generated. The WENO high-order numerical scheme is capable of computing both perfect air and equilibrium air flight conditions. The inviscid flow solver incorporates an equilibrium air curve fit formulation to account for flows involving the high temperatures encountered by hypersonic vehicles. The aerodynamic heating methods are capable of computing heating rates for both laminar or turbulent flows. They can use a constant entropy or variable entropy assumption. The heating methods are also capable of computing heating rates for both steady and transient flights.

Acknowledgments

This research was supported by the NASA Dryden Flight Research Center under Grant NCC 2-374. The authors thank Steven Speer of the University of California, Los Angeles, for his help in writing the paper and for producing some of the figures.

References

[1]Quinn, R. D., and Gong, L., "A Method for Calculating Transient Surface Temperatures and Surface Heating Rates for High-Speed Aircraft," NASA TP-2000-209034, Dec. 2000.

[2]Yamamoto, S., and Daiguji, H., "Higher-Order-Accurate Upwind Schemes for Solving the Compressible Euler and Navier–Stokes Equations," *Computers and Fluids*, Vol. 22, No. 2/3, 1993, pp. 259–270.

[3]Shu, C. W., and Osher, S., "Efficient Implementation of Essentially Non-Oscillatory Shock-Capturing Schemes," *Journal of Computational Physics*, Vol. 77, July 1988, pp. 439–471.

[4]Jiang, G. S., and Shu, C. W., "Efficient Implementation of Weighted ENO Schemes," *Journal of Computational Physics*, Vol. 126, No. 1, 1996, pp. 202–228.

[5]Harten, A., Engquist, B., Osher, S., and Chakravarthy, S., "Uniformly High Order Accurate Essentially Non-Oscillatory Schemes III," *Journal of Computational Physics*, Vol. 71, July 1987, pp. 231–303.

[6]Srinivasan, S., Tannehill, J. C., and Weilmuenster, K. J., "Simplified Curve Fits for the Thermodynamic Properties of Equilibrium Air," NASA Reference Publ. 1181, Aug. 1987.

[7]Grossman, B., and Walters, R. W., "Analysis of Flux-Split Algorithms for Euler's Equations with Real Gases," *AIAA Journal*, Vol. 27, No. 5, 1988, pp. 524–531.

[8]Grossman, B., and Walters, R. W., "Flux-Split Algorithms for the Multi-Dimensional Euler's Equations with Real Gases," *Computers and Fluids*, Vol. 17, No. 1, 1989, pp. 99–112.

[9]Eckert, E. R. G., "Survey of Heat Transfer at High Speeds," Wright Air Development Center, TR 54-70, Dayton, OH, April 1954.

[10]Eckert, E. R. G., "Survey of Boundary Layer Heat Transfer at High Velocities and High Temperatures," Wright Air Development Center, TR 59-624, Dayton, OH, April 1960.

[11]van Driest, E. R., "The Problem of Aerodynamic Heating," *Aerospace Engineering Review*, Vol. 15, No. 10, 1956, pp. 26–41.

[12]Zoby, E. V., Moss, J. N., and Sutton, K., "Approximate Convective Heating Equations for Hypersonic Flow," *Journal of Spacecraft and Rockets*, Vol. 18, No. 1, 1981, pp. 64–70.

[13]Quinn, R., and Palitz, M., "Comparison of Measured and Calculated Turbulent Heat Transfer on the X-15 Airplane at Angles of Attack up to 19.0," NASA TM X-1291, Sept. 1966.

W. E. Williamson
Associate Editor

Stagnation-Point Density of Hypersonic Ions in a Repelling Plasma Sheath

Ioannis G. Mikellides* and Myron J. Mandell†
Science Applications International Corporation, San Diego, California 92121
and
Ira Katz‡
Jet Propulsion Laboratory, California Institute of Technology, Pasadena, California 91109

Nomenclature

E	=	specific mechanical energy, J/kg
e	=	electron charge, C
f	=	velocity distribution function, s^3/m^6
$\boldsymbol{h}$	=	specific angular momentum vector, m^2/s
k	=	Boltzmann constant, J/K
M_0	=	Mach number of ions streaming with directed velocity $\boldsymbol{u}_0$
M_∞	=	Mach number of ions at infinity
m	=	ion mass, kg
n_i	=	ion particle density, m^{-3}
n_∞	=	ion particle density at infinity, m^{-3}
$\bar{n}$	=	ratio of local ion particle density to density at infinity
$\bar{n}_{\mathrm{NS}}$	=	ratio of stagnation density to density upstream of a normal shock wave
r	=	radius of orbiting ion, m
$\boldsymbol{r}$	=	position vector, m
T_e	=	electron temperature, K
T_i	=	ion temperature, K
$\boldsymbol{u}_0$	=	directed velocity of ions at zero electric potential, m/s
$\boldsymbol{u}_\infty$	=	velocity of ions at infinity, m/s
α_0	=	angle between directed ion velocity and axis of symmetry of hyperbolic orbit, rad
α_∞	=	angle between ion velocity vector at infinity with axis of symmetry of hyperbolic orbit, rad
γ	=	ratio of specific heats
ε	=	eccentricity of ion orbit
θ	=	polar angle in the spherical coordinate system (r, θ, Φ) measured with respect to $\boldsymbol{u}_0$ as polar axis, rad
μ	=	orbit constant, m^3/s^2
Φ	=	azimuthal angle in the spherical coordinate system (r, θ, Φ) measured with respect to $\boldsymbol{u}_0$ as polar axis, rad
φ	=	electric potential, V
χ	=	dimensionless electric potential
ψ	=	angle between ion velocity at infinity and ram ion velocity, rad

Introduction

AN important issue in simulating the environment around a low Earth satellite concerns the ram ions that stream toward the spacecraft. Much attention has been given to the wake that forms behind the spacecraft.[1–3] In this Note, we focus on the buildup of

Received 8 January 2002; revision received 16 August 2002; accepted for publication 16 September 2002.

*Senior Staff Scientist, Defense Technology Group, 9455 Towne Center Drive, Mail Stop W2076. Member AIAA.

†Senior Staff Scientist, Defense Technology Group, 10260 Campus Point Drive, Mail Stop X1. Senior Member AIAA.

‡Supervisor, Advanced Propulsion Technology Group, Thermal and Propulsion Engineering Section, 4800 Oak Grove Drive. Senior Member AIAA.

ion density in front of a spacecraft that is at a positive potential. Although most spacecraft surfaces in low Earth orbit are normally at negative potentials, positive potentials can be the result of electron beam emission, of being biased relative to a mother spacecraft, or of being at the upper end of a conductive tether. A repelling plasma sheath is formed that decelerates the ions as they approach the spacecraft, creating a region of enhanced ion density.

For simple cases (and if the spacecraft potential exceeds the mean ram ion energy), the maximum density occurs near a "stagnation point." To illustrate this better, consider the simplified one-dimensional case of collisionless, cold ions, $T_i = 0$, streaming toward a positively biased wall, $\varphi > 0$. Far from the wall, where $\varphi = 0$, the ions move with a uniform drift velocity $\boldsymbol{u}_0$. Conservation of energy and flux yields the ion density as a function of potential

$$\bar{n}(\varphi) \equiv n_i/n_\infty = 1\Big/\sqrt{1 - 2\chi\big/M_0^2} \tag{1}$$

where

$$\chi \equiv e\varphi/kT_e, \qquad M_0 \equiv |\boldsymbol{u}_0|\Big/\sqrt{kT_e/m} \tag{2}$$

Equation (1) shows that the ion density asymptotes to infinity at the stagnation point, where $\chi = M_0^2/2$. The asymptotic behavior of the density is analogous to the mathematical discontinuity encountered in the simplified modeling of supersonic flow over surfaces.[4] Although such idealized models provide useful information upstream and downstream of the shock wave, they provide no information on the variation of properties within the thin dissipative shock layer. Similarly, Eq. (1) does not capture the real continuous behavior of ion density in the plasma sheath and is, therefore, not realistic for spacecraft-environmenteffects studies.

A correct analytical determination of the ion density must take into account the distribution of ion velocities when $T_i \neq 0$. The high plasma density in low Earth orbit, and the resulting short Debye length make particle treatments impractical for obtaining self-consistent potentials, charge densities, and currents for realistic problems. Thus, potential calculations with charging codes such as NASCAP/LEO,[5] POLAR,[6] DynaPAC,[7] and Nascap-2K[8] usually invoke approximate analytic expressions for the charge density as a function of potential, electric field, and other available parameters.

The formulation leading to the determination of the species density begins with knowledge of the distribution function. If the spacecraft velocity is $-\boldsymbol{u}_0$, the distribution function for an ion of velocity $\boldsymbol{u}_\infty$ relative to the spacecraft, at a distance far from the spacecraft, is

$$f_\infty(\boldsymbol{u}_\infty) = n_\infty(m/2\pi kT_i)^{\frac{3}{2}}\exp\left[-(m/2kT_i)(\boldsymbol{u}_\infty - \boldsymbol{u}_0)^2\right] \tag{3}$$

Conservation of the distribution function along a trajectory allows the following mapping:

$$f(\boldsymbol{r}, \boldsymbol{u}) = f_\infty(\boldsymbol{u}_\infty) = n_\infty(m/2\pi kT_i)^{\frac{3}{2}}\exp\Big[-(m/2\pi kT_i) \times \left(u_\infty^2 - 2\boldsymbol{u}_\infty \cdot \boldsymbol{u}_0 + u_0^2\right)\Big] = n_\infty(m/2\pi kT_i)^{\frac{3}{2}} \times \exp\left\{-(M^2/2 + \chi) + M_0\sqrt{M^2 + 2\chi}\cos\psi - M_0^2/2\right\} \tag{4}$$

where $\chi = \chi(\boldsymbol{r})$ and the Mach numbers M and M_0 have been defined according to Eq. (2) using the ion temperature T_i. Integration of Eq. (4) over velocity space yields the ion density,

$$\bar{n}(\boldsymbol{r}) = \left(\frac{1}{2\pi}\right)^{\frac{3}{2}}\int_0^{2\pi} \mathrm{d}\Phi \int_0^{\pi} \sin\theta\,\mathrm{d}\theta \int_0^{\infty} \times \exp\left[-\frac{M^2}{2} - \chi + M_0\sqrt{M^2 + 2\chi}\cos\psi - \frac{M_0^2}{2}\right] M^2\,\mathrm{d}M \tag{5}$$

Results for Ion Density Profiles

In this section the ion density profile along the axis of a cylindrically symmetric problem is computed. Equation (5) now becomes

$$\bar{n}(\boldsymbol{r}) = \left(\frac{1}{2\pi}\right)^{\frac{1}{2}}\int_0^{1} \mathrm{d}v \int_0^{\infty} M^2\,\mathrm{d}M \times \exp\left[-\frac{M^2}{2} - \chi + M_0\sqrt{M^2 + 2\chi}\cos\psi - \frac{M_0^2}{2}\right] \tag{6}$$

where $v = \cos\theta$ and we have limited consideration to incoming particles only. The following cases will be presented: 1) planar or short-range potential (upper limit), 2) straight-line trajectories (lower limit), and 3) inverse-square potential. The three cases differ in the relation between $\cos\theta$ and $\cos\psi$.

A. Planar or Short-Range Potential

The planar potential case gives an upper limit to the maximum density because the incident ions are not deflected away from the axis. This treatment is also applicable to a potential whose range is small compared with its radius of curvature. The result may be derived directly from Eq. (6). An ion that passes through the axis must have only radial and axial velocity components, and in this case the radial velocity is conserved by the lack of any radial force. Thus, the relation between θ and ψ is

$$\boldsymbol{u}_{\perp,\infty} = \boldsymbol{u}_\perp \Rightarrow \sin\psi = |\boldsymbol{u}/\boldsymbol{u}_\infty|\sin\theta \tag{7}$$

or

$$\cos\psi = \sqrt{\frac{M^2\cos^2\theta + 2\chi}{M^2 + 2\chi}} \tag{8}$$

Defining $M_z = M\cos\theta$, Eq. (6) now becomes

$$\bar{n}(\boldsymbol{r}) = \left(\frac{1}{2\pi}\right)^{\frac{1}{2}}\int_0^{1} v^{-3}\,\mathrm{d}v \int_0^{\infty} M_z^2\,\mathrm{d}M_z \times \exp\left[-\frac{M_z^2}{2v^2} - \chi + M_0\sqrt{M_z^2 + 2\chi} - \frac{M_0^2}{2}\right] \tag{9}$$

The angular integral can be done by a change of variable to $w = 1/2v^2$, obtaining

$$\bar{n}(\boldsymbol{r}) = \left(\frac{1}{2\pi}\right)^{\frac{1}{2}}\int_0^{\infty} \mathrm{d}M_z \exp\left[-\frac{M_z^2}{2} - \chi + M_0\sqrt{M_z^2 + 2\chi} - \frac{M_0^2}{2}\right] \tag{10}$$

Figure 1 (solid curve) shows the resulting density for the case $M_0 = 9.7$, corresponding to a velocity of 7500 ms^{-1} and an ion temperature of 0.1 eV. The maximum density enhancement (by a factor of 2.3) occurs at a potential of 4 V, short of the ram ion energy of $E/e = 4.7$ V (assuming oxygen ions), which would normally be considered the stagnation point. Also, note that the calculation is for forward-moving ions only; if all ions are reflected, the densities would be twice as high everywhere suggesting that the true upper

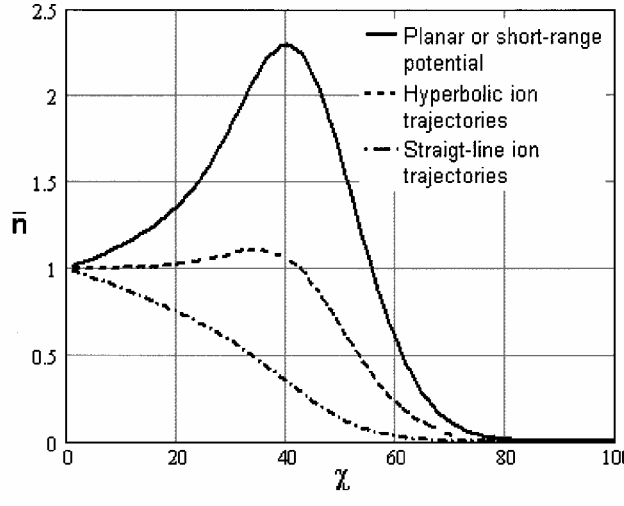

Fig. 1 Density enhancement factor for M_0 = 9.7 as a function of dimensionless potential.

limit maximum density enhancement factor is 4.6. However, in realistic cases, nonplanar forces cause high divergence of reflected ion trajectories, so that the reflected ions make only a small contribution to the density.

B. Straight-Line Trajectories

The approximation of straight-line trajectories, $\cos\psi = \cos\theta$, gives a lower limit to the density because, in reality, $\cos\psi \geq \cos\theta$ is always true. Using Eq. (6), the density is now given by

$$\bar{n}(r) = (2\pi)^{-\frac{1}{2}} \int_0^\infty \frac{M^2\,\mathrm{d}M}{M_0\sqrt{M^2+2\chi}} \exp\left[-\frac{1}{2}\left(M^2+2\chi+M_0^2\right)\right] \times \left\{\exp\left(M_0\sqrt{M^2+2\chi}\right)-1\right\} \tag{11}$$

The resulting density is shown in Fig. 1 (dash–dot curve). In this approximation, the density decreases monotonically with increasing potential. At the stagnation point the calculated density is only 0.2.

C. Hyperbolic Ion Trajectories

A more realistic case is when the ions move under the influence of a coulomb potential. Although this potential is longer ranged than a typical satellite sheath potential, this motion is well studied in the literature on such topics as planetary motion or Rutherford scattering (see Ref. 9). Figure 2 illustrates the geometry used to describe an ion trajectory in a $1/r^2$ force field. The objective in this section, i.e., the stagnation point, is to find the density at the point where the dashed line extending $\boldsymbol{u}_0$ intersects the dashed circle. The incoming ion will follow an orbit according to the equation of motion for the two-body problem. The orbit is a conic section (in polar coordinates):

$$r = \frac{h^2/\mu}{1+\varepsilon\cos\alpha_0} \tag{12}$$

where the (specific) angular momentum is simply $\boldsymbol{h} = \boldsymbol{r}\times\boldsymbol{u}$. The eccentricity of the orbit, ε, is

$$\varepsilon = \sqrt{1+2E(h/\mu)^2} = \sqrt{1+2\sin^2\theta(M^4/2\chi^2+M^2/\chi)} \tag{13}$$

with E the total (specific) energy, $E \equiv u^2/2 + e\varphi/m$. For a repelling potential ($e\varphi/m = \mu/r > 0$), the total energy is positive, and so the ion will follow a hyperbolic trajectory. As shown in Fig. 2, $\psi = \alpha_\infty - \alpha_0$. Using the properties of a hyperbola, the two angles α_∞ and α_0 can be expressed as functions of the eccentricity:

$$\pi - \alpha_0 = \cos^{-1}\{(-1/\varepsilon)[(M\sin\theta)^2/\chi + 1]\}$$
$$\pi - \alpha_\infty = \cos^{-1}(-1/\varepsilon) \tag{14}$$

When Fig. 2 is rotated by $2\alpha_0$, it can be seen that $\psi = \alpha_\infty + \alpha_0$ is the appropriate angle for calculating the density of outgoing particles.

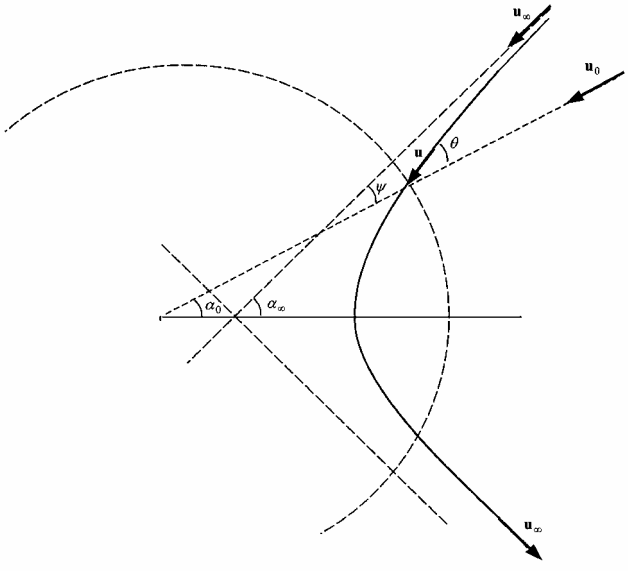

Fig. 2 Geometry used to calculate density for hyperbolic trajectory ions at the stagnation point.

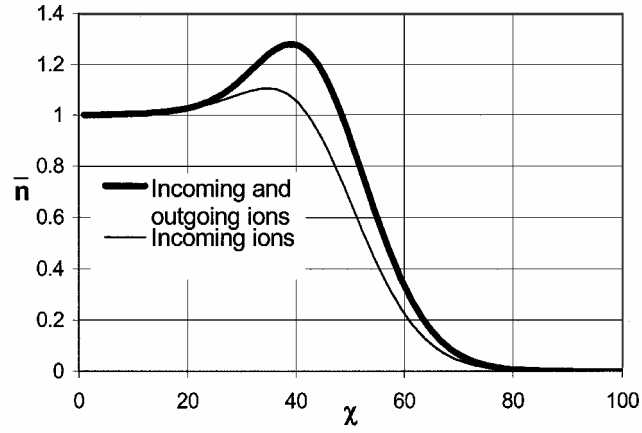

Fig. 3 Ion density enhancement in a coulomb potential for $M_0 = 9.7$ as a function of dimensionless potential χ.

Equations (14) can be implemented directly in Eq. (6) to compute the density at the stagnation point as a function of the electric potential. The result is plotted in Fig. 1 (dashed curve) for incoming ions only and in Fig. 3 for both incoming and outgoing ions, on numerical integration of Eq. (6).

The incoming ions show only a 10% density enhancement, with the maximum occurring well short of the stagnation point. Outgoing ions make a significant contribution to the density in the neighborhood of the stagnation point, bringing the density enhancement maximum up to 28%, but still at a potential of 4 V, well short of the expected stagnation point of $E/e = 4.7$ V. As a function of M_0, the maximum density (including reflected ions) is approximately

$$\begin{aligned} &1.0, && M_0 < 3 \\ &1.0 + 0.041(M_0 - 3), && M_0 > 3 \end{aligned} \tag{15}$$

Comparison with Continuum Fluid Flow

The low-density enhancement for hypersonic ions streaming through a $1/r^2$ force field contrasts strongly with stagnation densities achieved in collisional (low-Knudsen-number) hypersonic flows over surfaces. Clearly, the physics that determine density enhancement in the two regimes are very different. The driving mechanism in the deceleration of collisionless ions in the first case is the electric-potential force field. When an assumed velocity distribution as a function of distance from the body is used, then this force field was implicitly embedded in the formulations of the preceding sections. In this section, the simplified case chosen for comparison assumes no electric body forces, and, therefore, density enhancement is driven solely by the continuum (and, therefore, sufficient collisions to achieve equilibrium), gasdynamic conservation laws. When high-speed, continuum flows are obstructed by solid bodies, the mechanism that leads to density increase is a standing shock wave, which, in the absence of body forces, is governed solely by propagation of pressure disturbances, which is a purely collisional process. Even in the absence of any force fields, the conditions across a normal shock wave change as the collisionality of the ambient environment changes. For example, the density ratio across a normal shock may increase by almost a factor of two (for velocity ranges near and above orbital velocities) when the altitude (from sea level) at which the ratio is computed is increased from 10 to 100 km (Ref. 10). Consequently, in view of the inherently different underlying physics that govern density enhancement close to a hypersonic body, the benefit of comparing the two regimes must be taken as only educational at this point.

The determination of inviscid, supersonic flows over solid bodies is usually a numerically cumbersome task, even in the more simplified steady-state case because it involves the simultaneous solution of both elliptic and hyperbolic governing equations downstream of a detached shock wave. In certain ideal cases, such as one-dimensional, calorically perfect (constant γ), isentropic flow upstream and downstream of the shock, the solution is analytically traceable. The ratio of stagnation density to that upstream of the

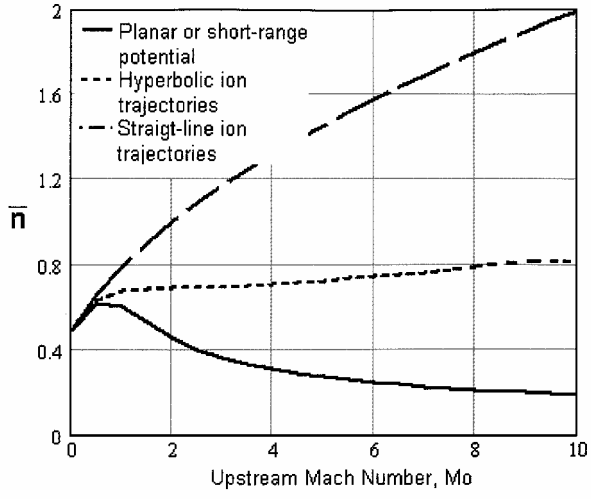

a)

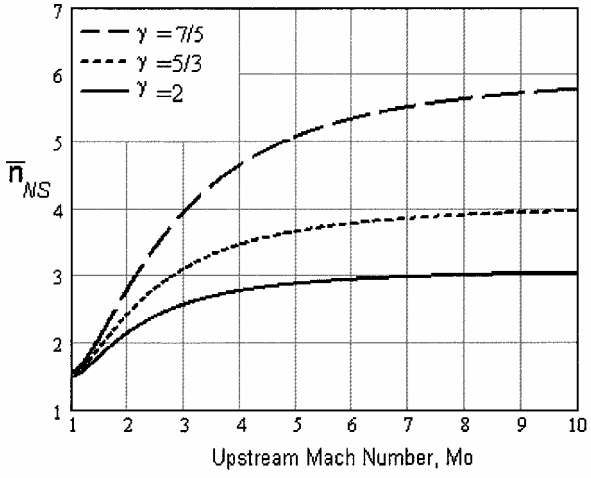

b)

Fig. 4 Density ratio at the stagnation point ($\chi = M_0^2/2$) as a function of a) upstream Mach number M_0 for free molecular flow (collisionless ions) and b) upstream Mach number for continuum, hypersonic flow across a normal shock wave.

shock in this case can be expressed as a function of the upstream Mach number[4]:

$$\bar{n}_{\mathrm{NS}} = \frac{(\gamma+1)M_0^2}{2+(\gamma-1)M_0^2}\left(1+\frac{\gamma-1}{2}\left\{\frac{1+[(\gamma-1)/2]M_0^2}{\gamma M_0^2-(\gamma-1)/2}\right\}\right)^{1/(\gamma-1)} \tag{16}$$

Equation (16) is plotted for different ratios of specific heats in Fig. 4b. By comparison, for a monatomic gas ($\gamma = \frac{5}{3}$) at $M_0 = 7$, the maximum density ratio is 3.86, which is by a factor of three larger than the peak density (1.16) computed by Eq. (15). At the stagnation point, $M_0 = \sqrt{(2\chi)}$, the density does not exceed unity for Mach numbers less than 10, as shown in Fig. 4a.

Conclusions

An integral expression for the density enhancement of hypersonic ions incident on a repulsive potential has been presented for the case of a $1/r^2$ force field, together with expressions for upper and lower limiting cases. For the interesting case of orbital velocity in a 0.1-eV oxygen plasma, deceleration of the incident ions produces a 10% density enhancement, whereas reflected (outgoing) ions contribute another 18%. The absolute upper enhancement for this case (planar potential with reflection) gives a factor of 4.6. The density maximum occurs at a potential of about 4 V, which is less than the ram ion energy of $E/e = 4.7$ V. The modest density enhancements calculated here are compared to density enhancement achieved in shocked hydrodynamic flows for which density ratios can exceed four at comparable Mach numbers.

Acknowledgment

This work is supported by Spectrum Astro, Inc., under Spectrum Astro Subcontract 01-057. (Prime Contract Number is F04071-C-0203.)

References

[1] Davis, V. A., Mandell, M. J., Cooke, D. L., and Enloe, C. L., "High-Voltage Interactions in Plasma Wakes: Simulation and Flight Measurements from the Charge Hazards and Wake Studies (CHAWS) Experiment," *Journal of Geophysical Research*, Vol. 104, No. A6, 1999, pp. 12,445–12,459.

[2] Biasca, R., and Wang, J., "Ion Current Collection in Spacecraft Wakes," *Physics of Plasmas*, Vol. 2, No. 2, 1995, pp. 280–289.

[3] Katz, I., Mandell, M. J., Parks, D. E., Wright, K., Stone, N. H., and Samir, U., "Effect of Object Potentials on the Wake of a Flowing Plasma," *Journal of Applied Physics*, Vol. 62, No. 3, 1987, pp. 2675–2686.

[4] Anderson, J. D., Jr., *Modern Compressible Flow*, 2nd ed., McGraw–Hill, New York, 1982, pp. 100–144.

[5] Mandell, M. J., and Katz, I., "High Voltage Plasma Interactions Calculations Using NASCAP/LEO," AIAA Paper 90-0725, Jan. 1990.

[6] Murphy, G., and Katz, I., "The POLAR Code Wake Model: Comparison with In-Situ Observations," *Journal of Geophysical Research*, Vol. 94, No. 5, 1989, pp. 9065–9072.

[7] Mandell, M. J., Luu, T., Lilley, J., Jongeward, G., and Katz, I., "Analysis of Dynamical Plasma Interactions with High Voltage Spacecraft," Maxwell Technologies, Rept. PL-TR-92-2258, San Diego, CA, June 1992.

[8] Mandell, M. J., Katz, I., Hilton, J. M., Minor, J., Cooke, D. L., "Nascap2k—A Spacecraft Charging Analysis Code for the 21st Century," AIAA Paper 2001-0957, Jan. 2001.

[9] Goldstein, H., *Classical Mechanics*, Addison–Wesley, Reading, MA, 1950, pp. 71–85.

[10] Anderson, J. D., Jr., *Hypersonic and High-Temperature Gas Dynamics*, McGraw–Hill, New York, 1989, pp. 507–520.

D. L. Edwards
Associate Editor

Rationale for Supersonic Afterburning Rocket Engines

G. E. Dorrington*
Queen Mary, University of London, London, England E1 4NS, United Kingdom

Nomenclature

g_0	=	gravitational acceleration at sea level, ms^{-2}
I_{spvac}	=	specific impulse (in vacuum), s
m_b	=	mass at burnout (main engine cutoff), kg
m_e	=	total main engine mass, kg
m_0	=	initial mass (at liftoff), kg
T_b	=	thrust at burnout (main engine cutoff), N
T_0	=	initial thrust (at liftoff), N
ΔV_{tot}	=	total delta-V requirement to attain orbit
μ	=	overall engine oxidizer/fuel-mass-flow-rate (mixture) ratio
μ_c	=	oxidizer/fuel-mass-flow-rate (mixture) ratio in chamber
ρ_{LH}	=	liquid hydrogen density, kg m^{-3}
ρ_{LOx}	=	liquid oxygen density, kg m^{-3}
ρ_p	=	bulk propellant density, kg m^{-3}
τ_e	=	main engine thrust-to-weight ratio, $T_0/(m_e g_0)$

Introduction

THE introduction of low-cost, commercial, reusable space transportation systems depends heavily on the appropriate

Received 27 August 2002; revision received 17 December 2002; accepted for publication 17 December 2002.

*Lecturer in Aerospace Design, Department of Engineering.